

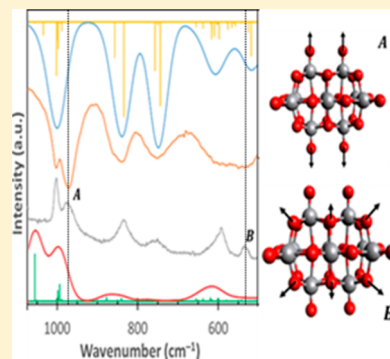
Features of Vibrational and Electronic Structures of Decavanadate Revealed by Resonance Raman Spectroscopy and Density Functional Theory

Paula F. Avila, Thomas J. Ripplinger, David J. Kemper, Joseph L. Domine, and Christopher D. Jordan*[✉]

Department of Chemistry, Saint Mary's University of Minnesota, 700 Terrace Heights, Winona, Minnesota 55987, United States

W Web-Enhanced Feature S Supporting Information

ABSTRACT: Polyoxometalates are known to be inhibitors of a diverse collection of enzymes, although the specific interactions that lead to this bioactivity are still unclear. Spectroscopic characterization may be an invaluable if indirect tool for remedying this problem, yet this requires clear, cogent assignment of polyoxometalate spectra before the complicating effect of their binding to large biomolecules can be considered. We report the use of FT-IR and resonance Raman spectroscopies alongside density functional theory to describe the vibrational and electronic structures of decavanadate, $[\text{V}_{10}\text{O}_{28}]^{6-}$. Our computational model, which reproduced the majority of vibrational features to within 10 cm^{-1} , was used to identify an axial oxo ligand as the most likely position of the acidic proton in the related cluster $[\text{HV}_{10}\text{O}_{28}]^{5-}$. As resonance Raman spectroscopy can directly interrogate chromophores embedded in complex systems, this approach may be of general use in answering structural questions about polyoxometalate–enzyme systems.



Over the last 3 decades, polyoxometalates (POMs) have attracted increasing attention due to their many applications, including as potent and selective inhibitors of an impressive variety of enzymes.^{1–5} POMs are metal-oxo clusters, the simplest of which contain ions of a single transition metal in its highest oxidation state (e.g., V^{5+} , W^{6+}) connected via bridging oxo ligands. While these POMs afford some structural variety, they can also be readily modified by functionalization of the outer oxo ligands and/or replacement of one or more metal ions with other d-block or main group elements.^{6–8} Thus, POMs possess an incredible diversity of charge, size, symmetry, electronic structure, magnetism, and other properties that are inaccessible to organic compounds.⁹ The vast chemical space covered by this class of compounds gives them immense potential as future therapeutics, which can be uniquely tailored to their biological targets. Indeed, in recent years, the biological activity of POMs, including their antibacterial^{10–12} and antimicrobial¹³ properties, has become a matter of intense scrutiny.

One obstacle toward the rational design of POM-based drugs is the poor characterization of the interactions between POMs and the enzymes that they inhibit. Due to the difficulty in obtaining structural data that reveal the binding geometry of these inhibitors, published structures are rare,^{3,14} and the effects of the protein on the POM's geometric and electronic structure are largely unknown. It is highly likely that association with an asymmetric proteinaceous binding pocket will introduce deformations to an otherwise highly symmetric POM structure. In the absence of crystal structures, spectroscopic data (from, e.g., ^{51}V NMR⁵ or EXAFS¹⁵ experiments) can provide indirect yet potentially insightful

descriptions of the POM's environment. Unlike most proteins, many POMs absorb visible light. Although the UV–visible absorption spectrum of a POM is itself of limited use, the underlying electronic transitions allow for the collection of a resonance Raman (rR) spectrum in which the chromophore's vibrational features are selectively enhanced over those of the protein. The vibrational spectra of a protein-bound POM should contain a plethora of information about the changes incurred to the inhibitor's structure, making rR spectroscopy a potentially useful technique for analyzing changes to a POM without unwanted background noise from the protein to which it binds.

In order to interpret these spectroscopic shifts, it is first necessary to have an accurate assignment of the POM's vibrational spectra. However, even relatively simple POMs, such as decavanadate ($[\text{V}_{10}\text{O}_{28}]^{6-}$, V_{10} , Figure 1), have intricate spectra with features that have not been assigned in detail. Accordingly, we synthesized ammonium decavanadate and collected its FT-IR spectrum and, for the first time, its rR spectrum. The former (Figure S1) is consistent with previously reported results.¹⁶ While the sharp feature at $\sim 1550\text{ cm}^{-1}$ is due to the ammonium counterion and the broad high-energy features are due to at least one O–H stretch (indicating protonation of one of the POM's exterior oxo ligands), the many overlapping features in the so-called “fingerprint region” cannot be assigned on the basis of this spectrum alone. Thus, we analyzed it alongside the rR spectrum in the 200–1200

Received: August 12, 2019

Accepted: September 20, 2019

Published: September 20, 2019

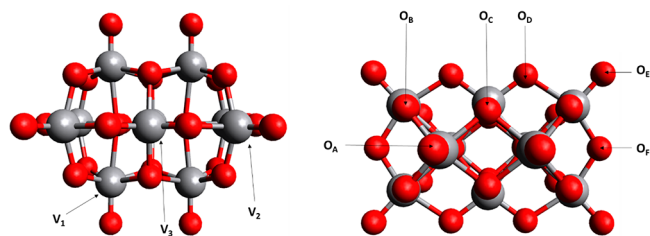


Figure 1. Ball-and-stick representation of the decavanadate ion, as seen from the side (left) and top (right). Labels for sets of symmetry-equivalent vanadium ions (gray) and oxo ligands (red) are included. Two oxo ligands (O_C) in the interior of the POM are unlabeled.

cm^{-1} range (Figure 2). Notably, each peak in the FT-IR spectrum was found to be slightly lower in energy than the corresponding rR feature, possibly due to collection of the former using solid KBr pellets at room temperature and the latter with an aqueous solution flash-frozen in liquid N_2 (see the [Experimental and Computational Methods](#) section). Accordingly, the rR spectrum in Figure 2 includes a uniform blue shift of 15 cm^{-1} . Because of the high resolution of the rR spectrum at low energy and the complementary nature of the two spectra, they allowed identification of 11 distinct transitions (Table 1).

To assign these features, we optimized the geometry of V_{10} at the PBE0/def2-TZVP^{17,18} level of theory and used the

resulting structure to compute the POM's FT-IR and Raman spectra. Figure 2 compares these spectra to their experimental counterparts and demonstrates excellent agreement between experiment and theory. The computed spectra predict 9 of the 11 features observed experimentally with a mean absolute error of less than 12 cm^{-1} (Table 1), with the exceptions of the pair of high-energy features at 972 and 1001 cm^{-1} , which will be discussed later. We note that these results are consistent with a previously reported simulated Raman spectrum, which was used to distinguish V_{10} from other vanadate oligomers (e.g., $[\text{V}_2\text{O}_7]^{4-}$, $[\text{V}_4\text{O}_{12}]^{4-}$) but was not otherwise discussed in detail.¹⁹

The strong performance of our computational model allowed us to use it to assign the vibrational spectra of V_{10} . Given the POM's high degree of symmetry and the number of bridging ligands, reducing each vibrational mode to a simple assignment is nontrivial. However, we find that high-frequency modes (700 cm^{-1} and higher) contain primarily V–O stretching character. At slightly lower frequencies, O–V–O and V–O–V bending motions are pronounced, with some fully delocalized, symmetric breathing modes represented in the Raman spectrum. Below 400 cm^{-1} , the high density of states and complicated normal modes preclude any meaningful assignment of features. Despite the complexity of these vibrations, we are encouraged by the ability of our computational methods to faithfully reproduce both the frequencies and the relative IR and Raman intensities.

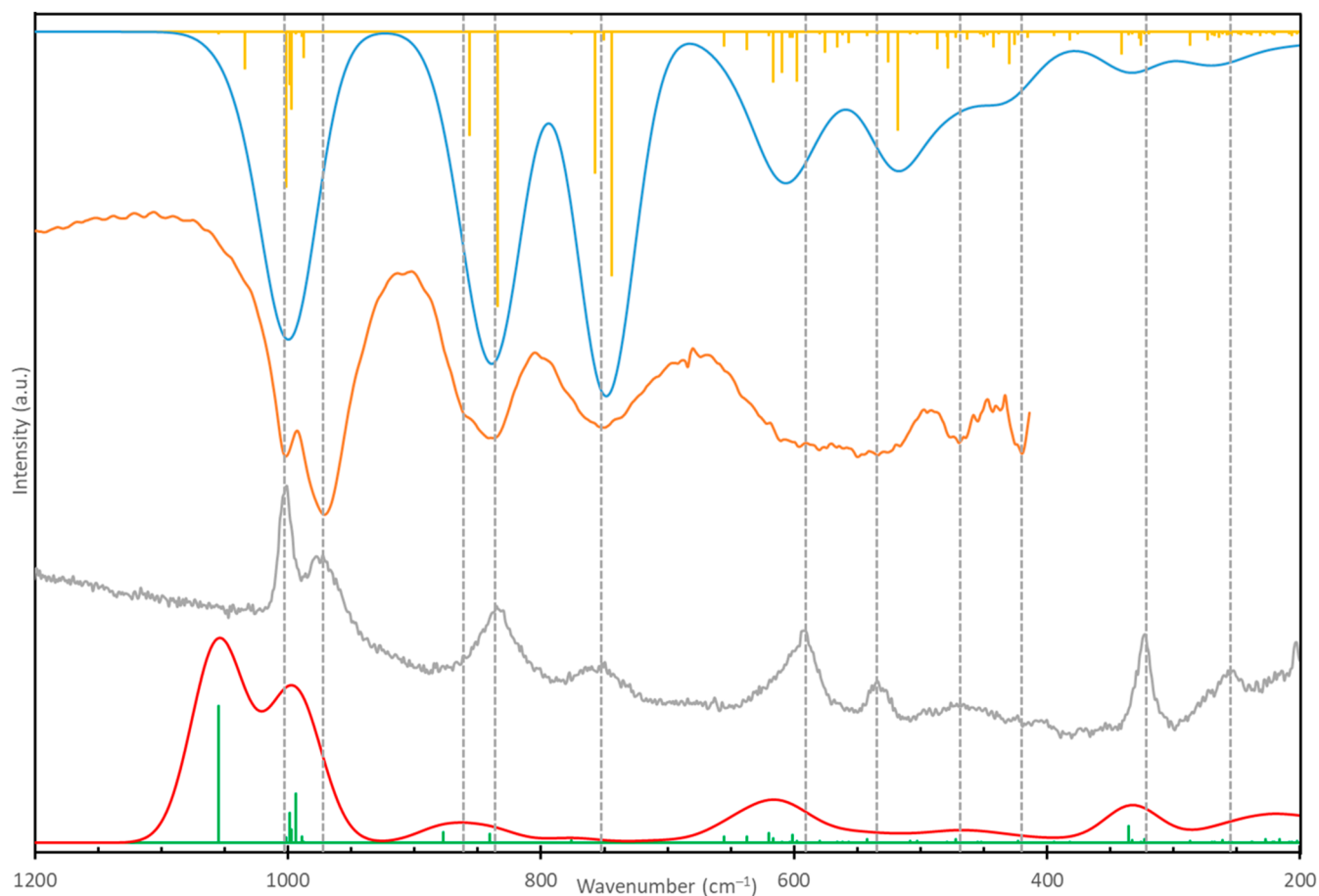


Figure 2. Experimental rR (gray) and FT-IR (orange) spectra and computed FT-IR (blue curve, yellow sticks) and Raman (red curve, green sticks) spectra of V_{10} . Vertical dashed lines indicate the positions of maximum Raman intensity or minima of FT-IR transmission in the experimental spectra. The spectra are offset vertically for clarity.

Table 1. Experimental and Predicted Vibrational Frequencies of Ammonium Decavanadate

experimental method	experimental energy (cm ⁻¹)	computed energy (cm ⁻¹)	difference (cm ⁻¹)	assignment ^a
FT-IR, rR	1001	1053 ^b	+52	V ₁ -O _A , V ₂ -O _E symmetric stretches
FT-IR, rR	972	997 ^b	+25	V ₁ -O _A symmetric stretch
FT-IR	854	857 ^{b,d}	+3	O _D -V ₃ -O _D symmetric stretch
FT-IR, rR	839	835 ^b	-4	O _D -V ₃ -O _D , V ₁ -O ₃ -V ₂ asymmetric stretches
FT-IR, rR	749	748 ^b	-1	V ₁ -O _B -V ₂ asymmetric stretch
rR	591	617 ^c	+12	O _F -V ₂ -O _G bends; V ₁ rocks
rR	534	541 ^{c,d}	+7	breathing
FT-IR, rR	470	478 ^c	+8	O _C -V ₃ -O _G bend
FT-IR	420	430 ^{b,d}	+10	O _G -V ₃ -O _G wag; V ₁ twists
rR	322	331 ^c	+9	
rR	251	261 ^b	+10	

^aAnimations for each assigned normal mode are available as web-enhanced objects 1, 2, and 3. ^bPosition determined with the computed FT-IR spectrum. ^cPosition determined with the computed Raman spectrum. ^dThe position of peaks that appear as shoulders in simulated spectra are identified with the frequency of the most intense transition that contributes to the feature.

This model represents an important step forward for the eventual biophysical application of vibrational spectroscopy to the problem of enzyme inhibition by POMs. While such applications are outside of the scope of the present work, we used our vibrational assignments to approach the question of the protonation of V₁₀. It has previously been established that under acidic conditions V₁₀ accepts one proton to form [HV₁₀O₂₈]⁵⁻, or HV₁₀.²⁰ While this is known to be the origin of the O-H stretch observed at ~3000 cm⁻¹ in the FT-IR spectrum of ammonium decavanadate, the site of protonation has not been conclusively determined.¹⁶

The presence of a proton suggests a plausible reason for the discrepancies between experimental and computational frequencies for the stretching modes at ~1000 cm⁻¹. That is, Figure 2 displays experimental spectra of HV₁₀ but computed spectra of V₁₀; despite their general agreement, the specific differences between them provide evidence of where the acidic proton binds to decavanadate. As the high-energy vibrational states in both the computed IR and rR spectra include V₁-O_A stretching character, we propose that the proton in HV₁₀ is bound to one of the four equivalent O_A ligands. To test this assignment, we optimized the proposed structure of HV₁₀ using the same computational methods as our other model (Figure S2) and computed its FT-IR spectrum. As expected, the conversion of an oxo ligand to a hydroxo ligand results in a significant increase of the corresponding V₁-O_A(H) bond length from 1.596 to 1.784 Å. The weak trans influence exhibited by the hydroxo ligand leads to a decrease in the V₁-O_G bond length, from 2.223 to 1.993 Å, a change that indirectly influences the entire POM geometry.

These changes in molecular structure also impact the computed FT-IR spectrum (Figure 3). While the spectra of V₁₀ and HV₁₀ are quite similar for transitions under 700 cm⁻¹, the loss of symmetry upon protonation changes the width and

appearance of higher-energy features. In particular, two low-energy shoulders are new to the HV₁₀ spectrum due to transitions at 718 cm⁻¹ (ν₉₉) and 976 cm⁻¹ (ν₁₁₀). Both of these features couple the V-O-H bend to motions of the POM. Meanwhile, the high-energy transitions at ~1000 cm⁻¹, assigned to the V₁-O_A stretch in V₁₀, show additional broadening in the HV₁₀ spectrum. This is consistent with the indirect distortions caused by protonation as the three unprotonated O_A ligands now have unique V₁-O_A bond lengths varying from 1.578 to 1.609 Å, resulting in a range of stretching frequencies. These observations (the presence of multiple peaks around 1000 cm⁻¹; the broadening of midrange features) are consistent with the experimental spectra of HV₁₀ (Figure 2).

Further evidence that O_A is the site of protonation comes from our model's description of the POM's electronic absorption spectrum. While to our knowledge we are reporting the first resonance Raman spectrum of V₁₀, others have reported its FT-Raman spectrum, acquired with an off-resonant excitation wavelength of 1024 nm.¹⁹ In both the off-resonant spectrum and our computed Raman spectrum (Figure 2, red trace), the V₁-O_A(H) stretching modes clearly have the highest Raman intensity, an order of magnitude higher than the peaks found at 750 cm⁻¹ and below. However, in our rR spectrum (Figure 2, gray trace), we find these features to be much more similar in intensity. This is consistent with TD-DFT calculations that we have performed, which predict the lowest-energy absorption feature to conceal a manifold of nearly degenerate electronic transitions (Figure S3). An electron density difference map (EDDM) of the most intense transition within this manifold identifies significant ligand-to-metal charge transfer character, consistent with the formal d⁰ electron configuration of the V⁵⁺ ions (Figure 4). Notably, the EDDM shows contributions from all oxo ligands except for O_A and O_E. The intensity of any mode is enhanced in rR spectroscopy only if the electronic transition at the excitation wavelength perturbs the potential energy surface along that coordinate. As the O_A-based molecular orbitals do not contribute significantly to the electronic transition, it is reasonable that the intensity of the V₁-O_A stretch will not show the same enhancement as the normal modes involving the other oxo ligands.

In summary, we have reported the rR spectrum of ammonium decavanadate for the first time. This spectrum, in conjunction with the FT-IR spectrum, was used to validate a theoretical model generated with density functional theory. This model was then used to assign major features in the experimental spectra, identify the previously unknown site of protonation in HV₁₀, and characterize the electronic transition probed in the rR experiment. The success of this combined theoretical and experimental approach strongly motivates similar study of enzyme-bound V₁₀. rR spectroscopy is particularly promising for this application because only V₁₀ vibrations—and not those of the protein itself—will couple to the electronic transition and show enhanced intensity. The specificity of rR spectroscopy allows for the targeted examination of the chromophore without generating noise from its environment. As such, this method is distinct from previous approaches that have used FT-Raman spectroscopy to identify secondary structural features with characteristic fingerprints.^{21,22} The rR spectrum presented in Figure 2 was produced from a ~3 mM solution, and its high resolution suggests that spectra could be collected for enzyme-bound V₁₀

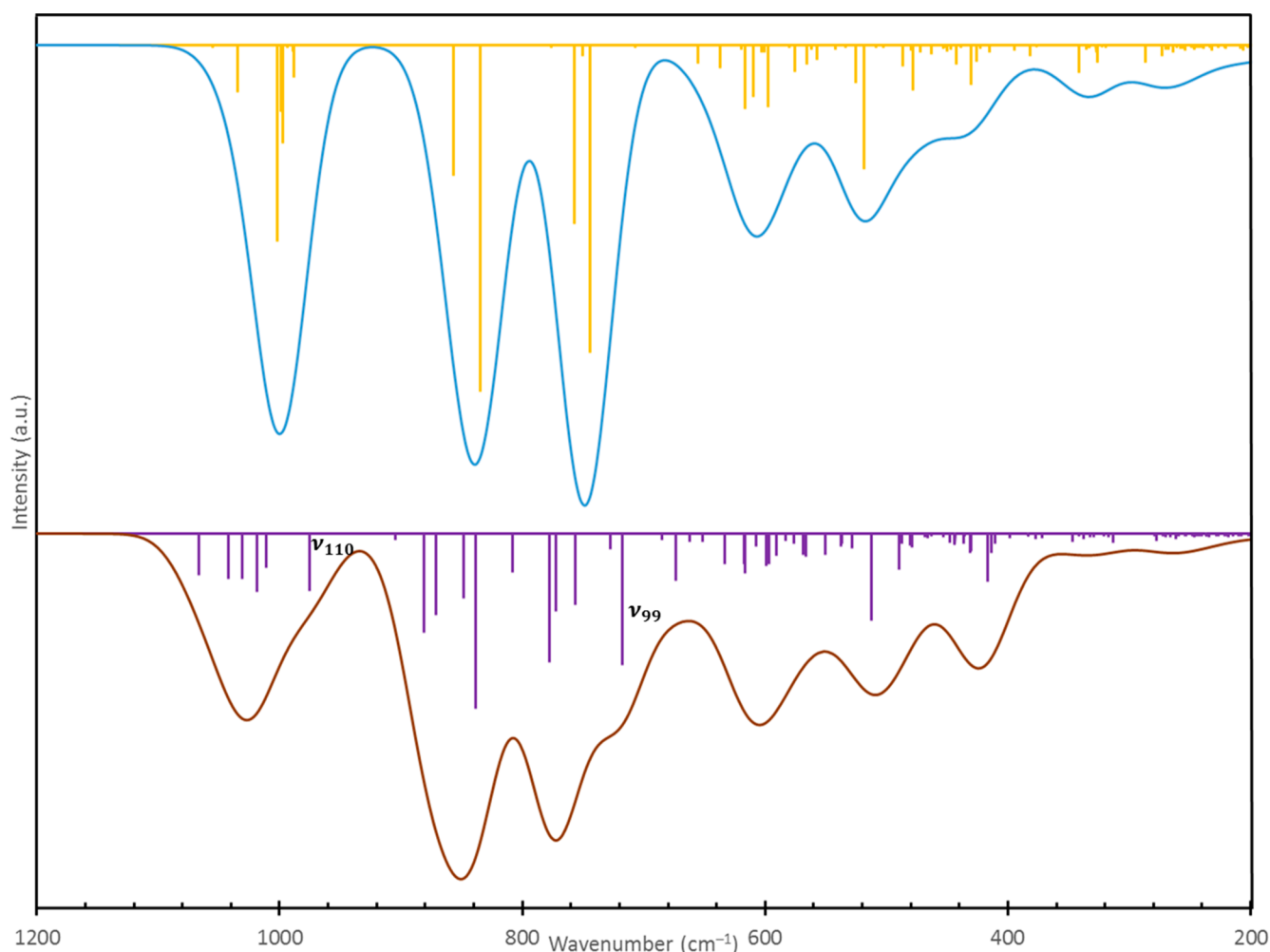


Figure 3. Computed FT-IR spectra of V_{10} (blue curve; yellow sticks) and HV_{10} (brown curve; purple sticks). The spectra are offset vertically for clarity. Features due to normal modes 99 and 110 in HV_{10} are identified and discussed in the text.

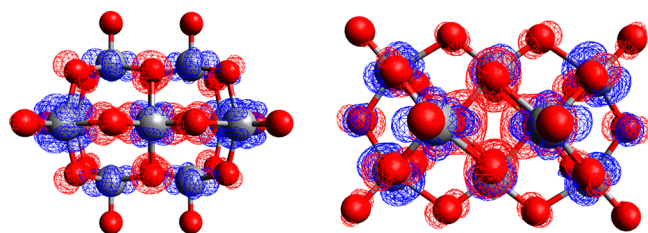


Figure 4. TD-DFT-computed EDDM of the highest-intensity electronic transition in the visible range of the V_{10} absorption spectrum. Regions shown with blue and red mesh indicate electron gain and loss during the transition, respectively.

even if lower concentrations are required. As a result of this work, any observed perturbations to the V_{10} rR spectrum that occur upon binding to a protein can be used to identify the portion(s) of the POM that directly interact with its target. Similarly, this information may also be used to test and validate atomistic models of the complete protein/POM complex.

EXPERIMENTAL AND COMPUTATIONAL METHODS

Ammonium decavanadate was synthesized by following the procedure of Sanchez-Lombardo et al.¹⁶ All materials were purchased from Sigma-Aldrich and used as supplied. In brief,

ammonium metavanadate (2.854 g) was dissolved in 22.5 mL of deionized water ($>2 \text{ m}\Omega\text{-cm}$). The pH of the solution was then lowered to ~ 3 by addition of 6 M HCl. Addition of 15 mL of 95% ethanol resulted in an orange–yellow precipitate that was isolated by vacuum filtration. An aqueous solution of the product ($\sim 4 \text{ mM}$) was characterized by electronic absorption spectroscopy using a Thermo Scientific Evolution 300 UV–vis spectrophotometer and a quartz cuvette with a 1 cm path length. A ^{51}V NMR spectrum (Figure S4) was also collected using a JEOL 300 MHz ECX NMR and found to be consistent with previous reports.¹⁶

Solid samples for FT-IR spectroscopy were prepared by pressing $\sim 0.05 \text{ g}$ of ammonium decavanadate into a KBr pellet; FT-IR spectra were collected by averaging eight scans with a Nicolet 380 FT-IR spectrophotometer. Samples for rR spectroscopy were made by flash-freezing drops of a 3.2 mM aqueous solution of ammonium decavanadate in liquid nitrogen to form frozen pellets. The pellets were kept in a finger dewar filled with liquid nitrogen for the duration of data collection. A COHERENT Inova Sabre DBW25 argon ion laser was used with an excitation wavelength of 485 nm. The laser power at the sample was 30 mW. Light scattered at a $\sim 135^\circ$ angle was dispersed by a triple monochromator (Acton Research SpectraPro) with a 1200 g/mm grating and detected

with a liquid-N₂-cooled CCD camera (Princeton Instruments Spec-100BR).

All computations were carried out using ORCA, version 4.0.0.2.²³ The geometry of decavanadate was initially optimized at the PBE0/def2-SVP level of theory, with the optimized structures further refined using the more robust def2-TZVP basis set. Vibrational frequencies and the polarizability tensor for the final structures were calculated at the same level, which was also used for the time-dependent DFT calculation of the V₁₀ absorption spectrum. In all computations, the conductor-like polarizable continuum model (CPCM)²⁴ was used to implicitly model an aqueous environment. Animations of key normal modes were visualized in Avogadro 1.2.0 in order to assign the vibrational spectra of V₁₀.²⁵

■ ASSOCIATED CONTENT

📄 Supporting Information

The Supporting Information is available free of charge on the ACS Publications website at DOI: 10.1021/acs.jpcclett.9b02362.

Experimental FT-IR and ⁵¹V NMR spectra of ammonium decavanadate and computed optimized geometry and electronic absorption spectrum of V₁₀ (PDF)

🌐 Web-Enhanced Feature

Animations for each assigned normal mode.

■ AUTHOR INFORMATION

✉ Corresponding Author

*E-mail: cdjordan@smumn.edu.

ORCID

Christopher D. Jordan: 0000-0002-2489-8244

Notes

The authors declare no competing financial interest.

■ ACKNOWLEDGMENTS

The authors are exceptionally grateful to Prof. Thomas Brunold and Mickie Killian (University of Wisconsin—Madison) for providing access to a resonance Raman laboratory and for assisting in data collection, and to Prof. Joseph West and the Department of Chemistry at Winona State University for providing access to NMR instrumentation.

■ REFERENCES

- (1) Stephan, H.; Kubeil, M.; Emmerling, F.; Mueller, C. E. Polyoxometalates as Versatile Enzyme Inhibitors. *Eur. J. Inorg. Chem.* **2013**, 2013 (10–11), 1585–1594.
- (2) Iqbal, J.; Barsukova-Stuckart, M.; Ibrahim, M.; Ali, S. U.; Khan, A. A.; Kortz, U. Polyoxometalates as Potent Inhibitors for Acetyl and Butyrylcholinesterases and as Potential Drugs for the Treatment of Alzheimer's Disease. *Med. Chem. Res.* **2013**, 22 (3), 1224–1228.
- (3) Arefian, M.; Mirzaei, M.; Eshtiagh-Hosseini, H.; Frontera, A. A Survey of the Different Roles of Polyoxometalates in Their Interaction with Amino Acids, Peptides and Proteins. *Dalton Trans* **2017**, 46 (21), 6812–6829.
- (4) Judd, D. A.; Nettles, J. H.; Nevins, N.; Snyder, J. P.; Liotta, D. C.; Tang, J.; Ermolieff, J.; Schinazi, R. F.; Hill, C. L. Polyoxometalate HIV-1 Protease Inhibitors. A New Mode of Protease Inhibition. *J. Am. Chem. Soc.* **2001**, 123 (5), 886–897.
- (5) Fraqueza, G.; Fuentes, J.; Krivosudsky, L.; Dutta, S.; Mal, S. S.; Roller, A.; Giester, G.; Rompel, A.; Aureliano, M. Inhibition of

Na(+)/K(+)- and Ca(2+)-ATPase Activities by Phosphotetradecavanadate. *J. Inorg. Biochem.* **2019**, 197, 110700.

(6) Zheng, S.-T.; Yang, G.-Y. Recent Advances in Paramagnetic-TM-Substituted Polyoxometalates (TM = Mn, Fe, Co, Ni, Cu). *Chem. Soc. Rev.* **2012**, 41 (22), 7623–7646.

(7) Kikukawa, Y.; Yokoyama, T.; Kashio, S.; Hayashi, Y. Synthesis and Characterization of Fluoride-Incorporated Polyoxovanadates. *J. Inorg. Biochem.* **2015**, 147, 221–226.

(8) Santoni, M.-P.; Pal, A. K.; Hanan, G. S.; Proust, A.; Hasenknopf, B. Discrete Covalent Organic-Inorganic Hybrids: Terpyridine Functionalized Polyoxometalates Obtained by a Modular Strategy and Their Metal Complexation. *Inorg. Chem.* **2011**, 50 (14), 6737–6745.

(9) Mjos, K. D.; Orvig, C. Metallo drugs in Medicinal Inorganic Chemistry. *Chem. Rev. (Washington, DC, U. S.)* **2014**, 114 (8), 4540–4563.

(10) Samart, N.; Arhouma, Z.; Kumar, S.; Murakami, H. A.; Crick, D. C.; Crans, D. C. Decavanadate Inhibits Mycobacterial Growth More Potently than Other Oxovanadates. *Front. Chem. (Lausanne, Switz.)* **2018**, 6, 519.

(11) Bijelic, A.; Aureliano, M.; Rompel, A. The Antibacterial Activity of Polyoxometalates: Structures, Antibiotic Effects and Future Perspectives. *Chem. Commun. (Cambridge, U. K.)* **2018**, 54 (10), 1153–1169.

(12) Marques-Da-Silva, D.; Fraqueza, G.; Lagoa, R.; Vannathan, A. A.; Mal, S. S.; Aureliano, M. Polyoxovanadate Inhibition of Escherichia Coli Growth Shows a Reverse Correlation with Ca2+-ATPase Inhibition. *New J. Chem.* **2019**, DOI: 10.1039/C9NJ01208G.

(13) Missina, J. M.; Gavinho, B.; Postal, K.; Santana, F. S.; de Souza, E. M.; Soares, J. F.; Nunes, G. G.; Valdameri, G.; Hughes, D. L.; Ramirez, M. I. Effects of Decavanadate Salts with Organic and Inorganic Cations on Escherichia coli, Giardia intestinalis, and Vero Cells. *Inorg. Chem.* **2018**, 57 (19), 11930–11941.

(14) Van Rompuy, L. S.; Parac-Vogt, T. N. Interactions Between Polyoxometalates and Biological Systems: From Drug Design to Artificial Enzymes. *Curr. Opin. Biotechnol.* **2019**, 58, 92–99.

(15) Marques, M. P. M.; Gianolio, D.; Ramos, S.; Batista de Carvalho, L. A. E.; Aureliano, M. An EXAFS Approach to the Study of Polyoxometalate-Protein Interactions: The Case of Decavanadate-Actin. *Inorg. Chem.* **2017**, 56 (18), 10893–10903.

(16) Sanchez-Lombardo, I.; Baruah, B.; Alvarez, S.; Werst, K. R.; Segaline, N. A.; Levinger, N. E.; Crans, D. C. Size and Shape Trump charge in Interactions of Oxovanadates with Self-Assembled Interfaces: Application of Continuous Shape Measure Analysis to the Decavanadate Anion. *New J. Chem.* **2016**, 40 (2), 962–975.

(17) Adamo, C.; Barone, V. Toward Reliable Density Functional Methods Without Adjustable Parameters: the PBE0Model. *J. Chem. Phys.* **1999**, 110 (13), 6158–6170.

(18) Weigend, F.; Ahlrichs, R. Balanced Basis Sets of Split Valence, Triple Zeta Valence and Quadruple Zeta Valence Quality for H to Rn: Design and Assessment of Accuracy. *Phys. Chem. Chem. Phys.* **2005**, 7 (18), 3297–3305.

(19) Aureliano, M.; Ohlin, C. A.; Vieira, M. O.; Marques, M. P. M.; Casey, W. H.; Batista de Carvalho, L. A. E. Characterization of Decavanadate and Decaniobate Solutions by Raman Spectroscopy. *Dalton Trans* **2016**, 45 (17), 7391–7399.

(20) Howarth, O. W.; Jarrold, M. Protonation of the Decavanadate-(6-) Ion: AVanadium-51 Nuclear Magnetic Resonance Study. *J. Chem. Soc., Dalton Trans.* **1978**, No. 5, 503–506.

(21) Fraqueza, G.; Batista de Carvalho, L. A. E.; Marques, M. P. M.; Maia, L.; Ohlin, C. A.; Casey, W. H.; Aureliano, M. Decavanadate, Decaniobate, Tungstate and Molybdate Interactions with Sarcoplasmic Reticulum Ca2+-ATPase: Quercetin Prevents Cysteine Oxidation by Vanadate but Does Not Reverse ATPase Inhibition. *Dalton Trans* **2012**, 41 (41), 12749–12758.

(22) Tuma, R. Raman Spectroscopy of Proteins: From Peptides to Large Assemblies. *J. Raman Spectrosc.* **2005**, 36 (4), 307–319.

(23) Neese, F. The ORCA Program System. *Wiley Interdiscip. Rev.: Comput. Mol. Sci.* **2012**, 2 (1), 73–78.

(24) Takano, Y.; Houk, K. N. Benchmarking the Conductor-like Polarizable Continuum Model (CPCM) for Aqueous Solvation Free Energies of Neutral and Ionic Organic Molecules. *J. Chem. Theory Comput.* **2005**, *1* (1), 70–77.

(25) Hanwell, M. D.; Curtis, D. E.; Lonie, D. C.; Vandermeersch, T.; Zurek, E.; Hutchison, G. R. Avogadro: an Advanced Semantic Chemical Editor, Visualization, and Analysis Platform. *J. Cheminf.* **2012**, *4*, 17.